Interfacial Phenomena and Heat Transfer, 1 (3): 215–230 (2013)

WETTING ON GELS: HOW THE GEL CHARACTERISTICS AFFECT THE CONTACT LINE DYNAMICS

Tadashi Kajiya,[1,*] Philippe Brunet,[1] Adrian Daerr,[1] Laurent Royon,[1] Tetsuharu Narita,[2] François Lequeux,[2] & Laurent Limat[1]

[1]*Laboratoire MSC, UMR 7057 CNRS, Université Paris Diderot, Bâtiment Condorcet, 10 rue Alice Domon et Léonie Duquet, 75205 Paris Cedex 13, France*

[2]*PPMD-SIMM, UMR 7615, CNRS, UPMC, ESPCIParisTech, 10 rue Vauquelin, 75231 Paris Cedex 05, France*

[*]Address all correspondence to Tadashi Kajiya, E-mail: tadashikajiya2@gmail.com

In this article, we summarize a series of experimental works and qualitative modelling regarding the dynamics of a liquid contact line on gel substrates. Two different situations were investigated, i.e., water on hydrophilic poly (2-acrylamido-2-methyl-propane-sulfonic acid-co-acrylamide) (PAMPS–PAAM) gels and water on hydrophobic poly (styrene-butadiene-styrene)(SBS)–paraffin gels. In both situations, different gel characteristics largely affect the contact line dynamics: liquid diffusion and surface deformation by capillary force. On hydrophilic gels, the contact line of a sessile droplet exhibits successively two different behaviors: pinned and receding, and the transition between the behaviors is closely related to the local deformation of the gel surface due to swelling. On hydrophobic gels, the contact line exhibits several different regimes of motions, i.e., stick-slip, and two continuous motions. These transitions are characterized by a frequency f built upon the apparent contact line velocity v and the droplet radius R as $f = v/R$, indicating that the gel rheology largely affects the dynamics of liquid contact line. Our results provide a synthetic view of the characteristic features of how the wetting is different on gel surfaces. Finally, we designate unsolved problems and future directions.

KEY WORDS: *A. wetting, gel, contact line, visco-elasticity*

1. INTRODUCTION

Gels are intriguing materials that behave either like solids or liquids due to three-dimensional cross-linked networks that expand throughout their entire volume by a fluid (Doi, 2009; Matsuo and Tanaka, 1992; Suzuki and Tanaka, 1990). Due to their unique properties, they have a large number of applications ranging from medical science to pharmaceutical and food chemistry (Hu et al., 2011; Peppas et al., 2000; Yang et al., 2005). For those applications, the key is the appropriate tuning of liquid/gel interfaces, as they determine adhesion and friction (Baumberger et al., 2006; Gong et al., 2001; Morishita et al., 2010) (e.g., cartilage replacement), surface tension, and wetting properties (e.g., soft contact lenses and artificial organs) (Kaneko et al., 2005; Nonomura et al., 2010, 2012; Szabó et al., 2000).

From the viewpoint of fundamental science, gels are interesting model systems for exploration of how liquid motion is different on surfaces which are not "ideal" solids. Statics and dynamics of wetting is still an active subject of research even on hard solid surfaces, as we have to consider the local balance of surface forces at the three-phase contact line in addition to classical hydrodynamics (Bonn et al., 2009; de Gennes et al., 2003). On gels, the situation would be more complex, as the wetting liquid can cause a large deformation on the gel surface which successively affects the statics and dynamics of the contact line. The gel deformation is caused by two mechanisms: by the balance between the interfacial tensions and elastic resistance of the gel and by the volume exchange between the liquid and gel (Banaha et al., 2009; Holmes et al., 2011). Intuitively, the behavior of the contact line on gels might be understood

2169–2785/13/$35.00

in analogy with the wetting on soft surfaces such as an elastomer (Carré and Shanahan, 2001; Lopes and Bonaccurso, 2012; Roman and Bico, 2010; Shanahan and de Gennes, 1986) or with the wetting on permeable surfaces such as porous media (Aradian et al., 2000; Bacri and Wyart, 2000). However, as gels have an unusual nature between solids and liquids, the wetting on gels would be even more complex than those situations (Daniels et al., 2007).

In this article, we summarize our experimental works and qualitative modelling regarding the contact line dynamics on gels in two different situations: water on hydrophilic gels (Kajiya et al., 2011) and on hydrophobic gels (Kajiya et al., 2013; Limat, 2012). In both situations, the different nature of gels affects the contact line dynamics.

As a first system, the dynamics of water sessile drops placed on hydrophilic poly(2-acrylamido-2-methyl-propane-sulfonic acid-co-acrylamide) (PAMPS–PAAM) gel substrates were studied. The precise analysis of the contact line in the presence of the substrate deformation and liquid diffusion requires measurement of both the profiles of the droplet and of the gel substrate simultaneously (Cámara et al., 2008, 2009). To obtain these two profiles, we used a "grid projection method" (Fermigier et al., 1992; Kurata et al., 1990), i.e., we projected a grid pattern below the gel surface and measured its optical distortion to reconstruct the original profile. We observed that as the water droplet diffuses into the gel substrate, the behavior of the contact line exhibits successively two different regimes, pinned and receding, and the transition between these two regimes is closely related to the local swelling of the gel around the contact line. We discuss how this pinned–receding transition depends on the gel properties, i.e., the rigidity and hydrophilicity (tuned by the concentrations of crosslinking agent and of hydrophilic AMPS monomer).

The other aspect of the gel complexity is the rheology. As a second system, we studied the dynamics of the moving contact line on poly(styrene-butadiene-styrene)(SBS)-paraffin gel substrates in two geometries: advancing drops and dip coating. As the SBS–paraffin gel is hydrophobic and there is no volume exchange between the drop and gel, the sole possible effect affecting the contact line is the gel surface deformation due to the capillary force of liquid (Carré and Shanahan, 2001; Shanahan and de Gennes, 1986) moderated by the viscoelastic response of the material. However, unlike the case of wetting on elastomer, the contact line exhibits quite complex behaviors, i.e., it shows two regimes of continuous advancing motion and one of stick-slip motion. The stick-slip motion of the contact line was previously observed by Pu et al. during the wetting on thin polymer films (Pu and Severtson, 2008; Pu et al., 2010). Here we found that on a SBS-paraffin gel, there are three different regimes, i.e., continuous, stick-slip, and another continuous motion. We discuss how the transitions of these contact line motions are characterized by the parameters, such as the frequency of the contact line motion, and propose a qualitative modelling.

2. WATER DROPS ON HYDROPHILIC GELS: EFFECT OF LIQUID DIFFUSION

2.1 Experiment

PAMPS–PAAM gels were used for the substrate, and distilled water (Milli-Q Integral; Millipore, USA) was used for liquid drops. The PAMPS–PAAM gels were prepared through the radical polymerization of a solution of 2-acrylamido-2-methyl-propane-sulfonic acid (AMPS; Sigma-Aldrich, USA) and acrylamide (AAM; Alfa Aesar, USA) in water with a crosslinking agent, N, N'-methylenebisacrylamide (MBA; Sigma-Aldrich, USA), and initiators, potassium persulfate (PS; Sigma-Aldrich, USA) and N, N, N', N'-tetramethylenediamine (TEMED; Sigma-Aldrich, USA). The total molar concentration of monomer was fixed at 1 M. The concentrations of AMPS and of crosslinking agent MBA with respect to the total amount of monomer were tuned as control parameters. The dimensions of the gel samples were 70 mm in length, 20 mm in width, and 4.5 mm in thickness.

Figure 1(a) shows the setup for the drop–gel profile measurement. The gel substrate was placed on a hollow stage, and a droplet of 1 μl volume was placed on the substrate with a micropipet. To measure both the profiles of the droplet and of the gel simultaneously, a grid projection technique was used (Fermigier et al., 1992; Kurata et al., 1990). In this technique, the profiles are obtained by tracing the distortion of grid lines between before and after the placement of the droplet. The original grid plate was located far from the observation system. The illumination light emitted from the photodiode passed through the grid plate and was converted to a parallel light by an optical lens (f = 200 mm). Then the light was guided to the bottom of the substrate and passed through a focus lens (TV lens f = 35 mm: Pentax, Japan). This focus lens projects the image of the grid inside the gel substrate, which is set just below the droplet. The

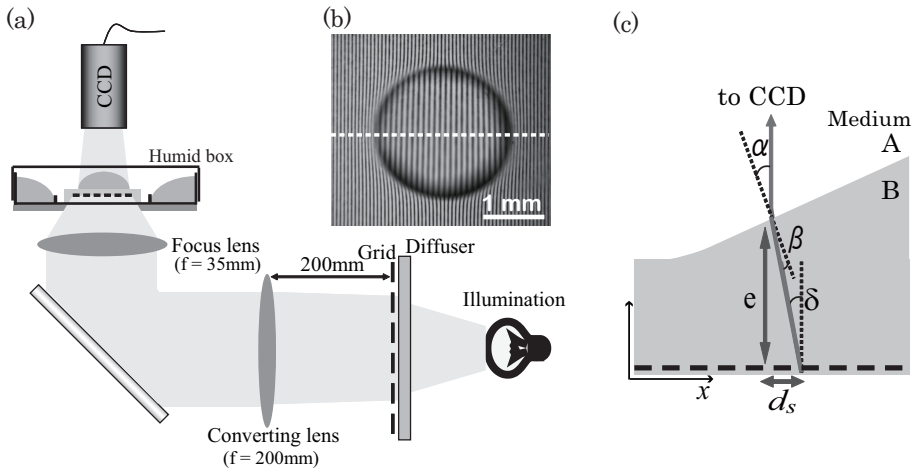

FIG. 1: (a) Schematic of grid projection technique method to obtain drop–gel profiles. **(b)** Example of the image of grid lines which is taken after the droplet is placed on the gel surface. **(c)** Geometry of the light path that passes the grid image and is detected by the CCD.

grid image was measured by a CCD camera (A101FC; Basler AG, Germany) which was located above the droplet. The example of the grid image obtained after the placement of the droplet is also shown in Fig. 1(b).

The original profile was reconstructed by tracing the light path which passes through each grid line. As shown in Fig. 1(c), the shift of the grid line d_s is related to the local slope of the interface between the media of different refraction ratios (medium A: air, medium B: water or gel). The relation between the shift and slope is given by the following three equations:

$$\sin \alpha = n \sin \beta, \tag{1}$$

$$\delta = \alpha - \beta, \tag{2}$$

$$\tan \delta = \frac{d_s}{e}, \tag{3}$$

where α and β are the angles of the light path in media A and B with respect to the normal to the interface, δ is the angle of the light path in medium B with respect to the vertical axis, and n is the refractive index of medium B (since the water volume fraction in the gel is considerably large, we used the value of water n = 1.33). By solving Eqs. (1)–(3), the local slope of the interface was obtained from d_s, and the whole profile was obtained by integrating in a horizontal direction x.

2.2 Results

Figure 2(a) shows the half cross sections of the profiles (height h against the radial position r) of the droplet and gel substrate at different times (substrate: C_{MBA} = 5 mol % and C_{AMPS} = 30 mol %). During the diffusion process of the droplet into the gel substrate, both the profiles of the droplet and substrate change. At an early stage (t = 25 s), the contact line of the droplet is seen clearly, i.e., the slope of the profile is discontinuous at the droplet perimeter. As the water diffusion proceeds, the height of the droplet decreases, while the height of the gel substrate around the contact line increases. The horizontal extent of the substrate deformation grows close to the order of 1 mm from the initial position of the contact line, and the boundary between the droplet and substrate becomes less clear.

At a late stage, we detected the position of the contact line using the local curvature of the profile at the center ($r \approx 0$). When a water droplet still remains on the gel surface, the surface of the center where the droplet resides must be a spherical cap of uniform curvature. Therefore, if the local curvature at the center H_c is calculated as

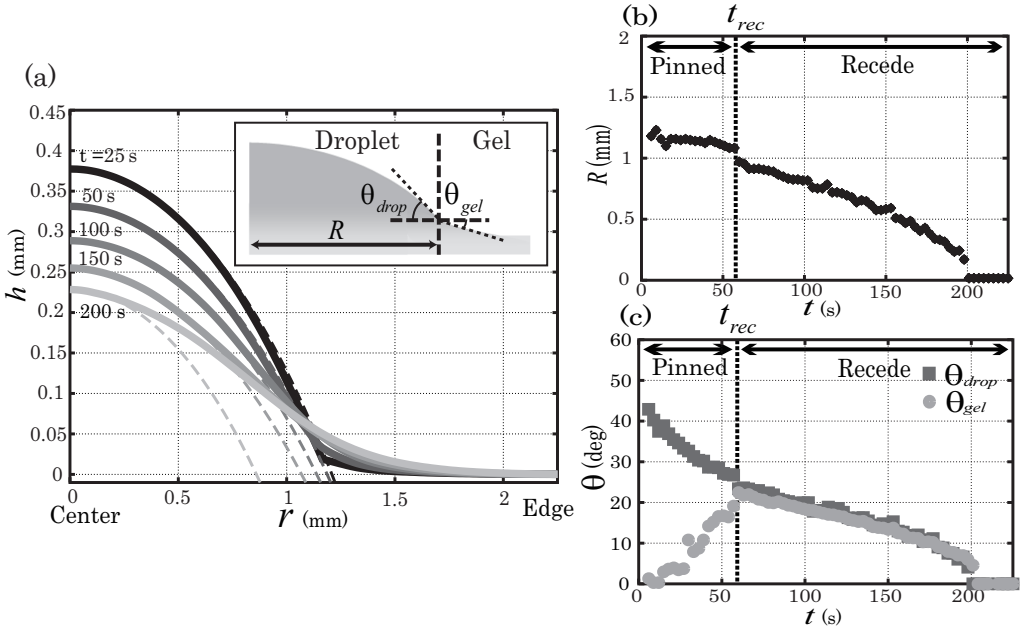

FIG. 2: (a) Half cross sections of the profiles of the droplet and substrate (C_{MBA} = 5 mol %, C_{AMPS} = 30 mol %) at t = 25, 50, 100, 150, and 200 s. To detect the position of the contact line, the extrapolations of the local curvatures at the center H_c are superposed as dashed lines. **(b)** Plot of the radius R against time t. **(c)** Plot of the angles of the droplet θ_{drop} and gel substrate θ_{gel} against t. The MBA concentration C_{MBA} is fixed at 5 mol %.

$$\frac{1}{H_c} \approx \frac{\partial^2 h}{\partial r^2}\Big|_{r\approx 0} \tag{4}$$

and is extrapolated outward, the contact line can be detected as the point where the actual profile deviates from the extrapolated H_c curve. The extrapolated H_c curves are also plotted in Fig. 2(a) as dashed lines.

Now that the position of the contact line has been detected, it is possible to measure the radius of the droplet R, the effective contact angle of the droplet θ_{drop} with respect to horizontal, and the angle of the local slope of the gel surface θ_{gel} close to the contact line. [The determination of R, θ_{drop}, and θ_{gel} are illustrated in the inset of Fig. 2(a).] Figure 2(b) shows the plot of R against time t, and Fig. 2(c) shows the plot of θ_{drop} and θ_{gel} against t. In both figures, the data of substrates C_{AMPS} = 30 mol % and C_{MBA} = 5 mol % are shown.

The behavior of the contact line exhibits two different regimes. The contact line is initially pinned, then at a time $t = t_{rec}$, it starts receding until the droplet has totally diffused into the gel. By comparing Fig. 2(b) with 2(c), it is clearly observed that the transition of the pinning to receding regimes is closely related to the variation of the angles θ_{drop} and θ_{gel}. At the initial stage where the contact line is pinned, the values of θ_{drop} and θ_{gel} are largely different. As the water diffusion proceeds, these two angles come close to each other: θ_{drop} decreases while θ_{gel} increases. At the moment where θ_{drop} and θ_{gel} almost correspond, the contact line starts to recede. This result indicates that when a contact line recedes on a PAMPS–PAAM hydrogel, apparently it has a finite receding contact angle, but the actual receding angle on the deformed gel surface $\theta_{drop} - \theta_{gel}$ is nearly 0°. The same trend was observed for all AMPS and MBA concentrations in our experiment.

We also explored how the pinned–receding transition of the contact line depends on the following parameters: the MBA concentration C_{MBA} that determines the rigidity of the gel substrate and the PAMPS concentration C_{AMPS} that determines the hydrophilicity of the substrate. In Fig. 3(a), we plot the relative ratio of initial pinning time to the total diffusion time t_{rec}/t_f on gels of various C_{MBA} and C_{AMPS}. For both C_{AMPS}, t_{rec}/t_f becomes longer with the increase of C_{MBA}, i.e., the contact line is pinned for a longer time as the gel becomes more rigid. Comparing the

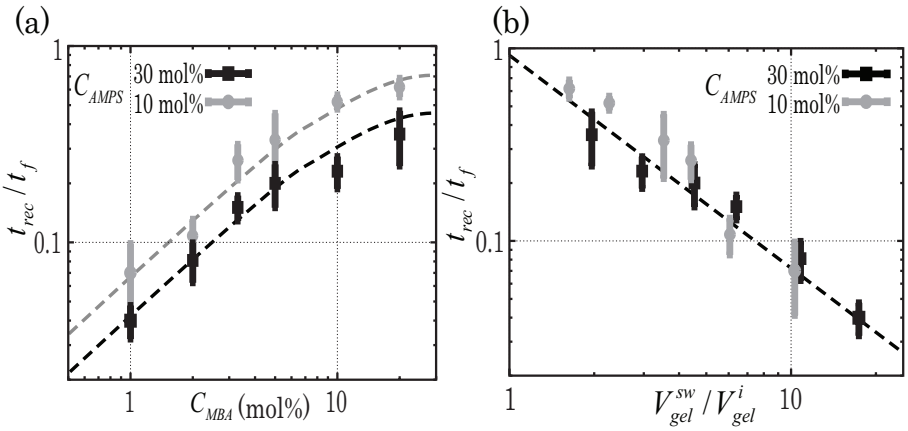

FIG. 3: (a) Plot of the relative pinning time to the total diffusion time t_{rec}/t_f against C_{MBA}. Data of two different C_{AMPS} (10 and 30 mol %) are plotted with different symbols. **(b)** Replot of t_{rec}/t_f against the volume swelling ratio V^{sw}_{gel}/V^{i}_{gel}.

data of different C_{AMPS}, t_{rec}/t_f is shorter for higher C_{AMPS} (30 mol %) in a whole range of C_{MBA}, indicating that the contact line recedes earlier when the gel substrate has higher hydrophilicity.

Indeed, both the parameters C_{MBA} and C_{AMPS} largely affect the swelling ability of the gel, i.e., the volume swelling ratio V^{sw}_{gel}/V^{i}_{gel}, where V^{sw}_{gel} corresponds the volume of the gel at the fully swollen state and V^{i}_{gel} the volume at the initial state. Considering that, the data t_{rec}/t_f for all gels are replotted as a function of V^{sw}_{gel}/V^{i}_{gel} in Fig. 3(b). It is clearly observed that t_{rec}/t_f has a universal negative dependence upon V^{sw}_{gel}/V^{i}_{gel}.

2.3 Discussion

In this section, we discuss why the actual contact angle of the droplet $\Delta\theta = \theta_{drop} - \theta_{gel}$ becomes nearly 0° at the moment of the contact line recession. Figure 4 shows the schematics of the mechanism we propose.

After the droplet is placed on a gel substrate, the water starts to diffuse from the droplet into the substrate, and the gel deforms as it swells with water. Here, we consider the diffusion of water into the gel with an analogy of the drying problems of the droplet (Deegan et al., 2000; Hu and Larson, 2002; Kobayashi et al., 2010). Due to the geometrical effect, it is expected that the diffusive flux of water near the edge of the droplet is largely enhanced compared to the center [Fig. 4(a)]. Therefore, the gel surface below the contact line swells with water rapidly, forming a "locally

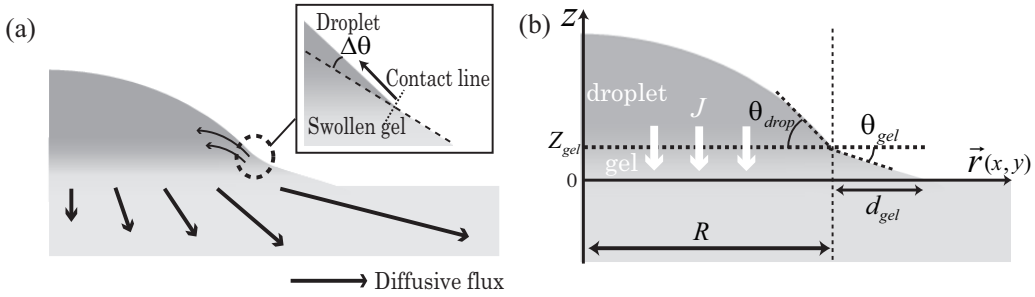

FIG. 4: (a) Mechanism of the recession of contact line. Contact line feels the locally swollen gel surface formed by diffusion of liquids. **(b)** Geometry and coordinates for the theoretical modelling.

swollen" region. For the contact line to recede, the actual contact angle of the droplet $\Delta\theta = \theta_{drop} - \theta_{gel}$ must correspond to the equilibrium contact angle on the swollen gel surface.

To check the wetting property of the swollen gel surface, we conducted a supplemental wetting experiment on a gel substrate which is previously fully swollen in a water bath. We observed that on a fully swollen gel, the droplet spreads rapidly and the contact angle takes a considerably small value ($< 3^\circ$) irrespective of C_{MBA} and C_{AMPS}. The results of the supplemental experiment imply that the equilibrium contact angle on the locally swollen gel surface is very close to 0°. This is consistent with the result that the contact line of the droplet is pinned until $\Delta\theta$ reaches nearly 0°.

The negative dependence of t_{rec}/t_f on the volume swelling ratio of the substrate V_{gel}^{sw}/V_{gel}^{i} in Fig. 3(c) can be understood in terms of the growth of the deformation of the gel surface. For a gel substrate with a large swelling ratio, the gel is highly permeable to water. After a droplet is placed on the substrate, water permeates into the gel rapidly and the regions near the water–gel interface are swollen by the flux, which causes the large rise of the gel surface around the droplet. Therefore, the local slope of the gel surface at the contact line θ_{gel} increases up to the value of θ_{drop} at an early stage of the diffusion process. On the other hand, for a gel with a small swelling ratio, the gel exhibits low permeability and thus the surface deformation by swelling is tiny. In that case, θ_{drop} does not correspond to θ_{gel} until the droplet diffuses most of water into the gel and decreases θ_{drop} to a small value.

To get the order of magnitude for θ_{drop} and θ_{gel} at the initial pinned-contact-line stage, we propose a simple model depicted in Fig. 4(b). We assume that below the droplet, the water diffusion creates the diffusive boundary layer of typical thickness $\sqrt{Dt}$, where D is the diffusion coefficient of water in the gel. The typical volume flux of water at the water–gel interface $z = z_{gel}$ is scaled as

$$J \sim D\frac{\phi_{sw} - \phi_i}{\sqrt{Dt}}, \tag{5}$$

where ϕ_{sw} is the volume fraction of water in the fully swollen gel (suppose that at the water–gel interface, gel is immediately swollen), and ϕ_i is the volume fraction of water in the gel at the initial state. Due to this flux, the volume of the droplet $V_{drop} \approx \pi R^3 \theta_{drop}$ decreases as

$$\frac{dV_{drop}}{dt} \approx \pi R^3 \frac{d\theta_{drop}}{dt} = -\pi R^2 J, \tag{6}$$

while the volume of the gel increases as

$$\frac{dV_{gel}}{dt} \approx \pi R^2 \frac{dz_{gel}}{dt} = \pi R^2 J. \tag{7}$$

The local slope of the gel near the contact line θ_{gel} is estimated to be close to the ratio z_{gel}/d_{gel}, where z_{gel} designates the vertical displacement of the droplet basis due to swelling, and d_{gel}, the horizontal distance on which this displacement relaxes radially around the droplet. With an analogy of a contact problem of solid bodies (Landau and Lifshitz, 1986), here we assume that the shape of the gel surface is mainly dictated by a compromise between the shear elasticity of the gel and the rising condition $z = z_{gel}$ at the droplet basis of radius R. The characteristic size of d_{gel} is thus estimated as the same order of the droplet radius: $d_{gel} \sim R$.

Combining Eqs. (5)–(7), the time evolution of the angles θ_{drop} and θ_{gel} are obtained as

$$\theta_{drop}(t) - \theta_{drop}^{(0)} \sim -\frac{\phi_{sw} - \phi_i}{R}\sqrt{Dt}, \tag{8}$$

$$\theta_{gel}(t) \sim \frac{\phi_{sw} - \phi_i}{R}\sqrt{Dt}, \tag{9}$$

where $\theta_{drop}^{(0)}$ is the initial value of the effective contact angle of the droplet. Equations (8) and (9) predict that the time evolutions of $\theta_{drop}(t) - \theta_{drop}^{(0)}$ and of $\theta_{gel}(t)$ are proportional to $\sqrt{t}$. From Eqs. (8) and (9), the characteristic time

of the contact line recession τ, i.e., the time when the actual contact angle $\Delta\theta = \theta_{drop} - \theta_{gel}$ goes to zero, is thus estimated as

$$\tau \sim \frac{(R\theta_{drop}^{(0)})^2}{D(\phi_{sw} - \phi_i)^2}. \tag{10}$$

Let us calculate τ for our gel (C_{MBA} = 5 mol %, C_{AMPS} = 10 mol %): R = 1.42 mm, $\theta_{drop}^{(0)}$ = 27.1°, $\phi_{sw} - \phi_i$ = 0.0529 (obtained by the measurement of swelling ratio), and D = 39.47 $\times$ 10^{-8} m^2/s [cited from Kundakci et al. (2008)]. By substituting these values in Eq. (10), τ is calculated as ca. 400 s. Experimentally, the time for the onset of the contact line recession was measured as 140 s, which is not far from our theoretical estimation.

3. MOVING CONTACT LINE ON HYDROPHOBIC GELS: EFFECT OF VISCOELASTOCAPILLARY DEFORMATION

3.1 Experiment

SBS–paraffin gels were used for the gel substrates and distilled water (Milli-Q Integral; Millipore, USA) was used for the liquid. SBS powders (G1682; Kraton Polymers, USA) were dissolved in paraffin (Norpar15; ExxonMobil, USA) heated in a water bath at 90°C. After SBS powders were completely dissolved, the solution was poured into a gel mold and was cooled down to ambient temperature. The mass concentration of SBS c_{SBS} was varied from 8% to 25%. The gel mold consists of two glass plates separated by a rubber spacer. The dimensions of the gel samples were 70 mm in length, 20 mm in width, and 2 mm in thickness. The rheology of the gel was measured by a strain-controlled rheometer (Physica MCR 500; Anton Paar, Austria). Shear strain amplitude was set to 1%, and the experiments were conducted at frequencies from 10^{-4} Hz to 10 Hz.

Figure 5(a) shows a schematic of the inflation experiment of a water droplet on the gel. A water droplet was placed on a gel by a microsyringe. The syringe was connected to a motor syringe pump (model 33; Harvard Apparatus, USA), and it supplies water to the droplet and inflates it at a constant volume rate q. From the side and top of the droplet, the shape of the droplet was monitored by two CCD cameras (model A101fc and model PLA1000; Basler, Germany) with magnification lenses (CCTV lens; Pentax, Japan).

We investigated the contact line dynamics in another geometry, a dip-coating experiment [see Fig. 5(b)] that allows an accurate control of the mean receding velocity and operation with a two-dimensional contact line. In the dip coating, the gel substrate was mounted on a translation stage and withdrawn from a liquid bath at a constant translation velocity v. The front view of the contact line and the side view of the meniscus was monitored by two CCD cameras. To enable the visualization of the meniscus, the stage was inclined at 15° against the vertical axis.

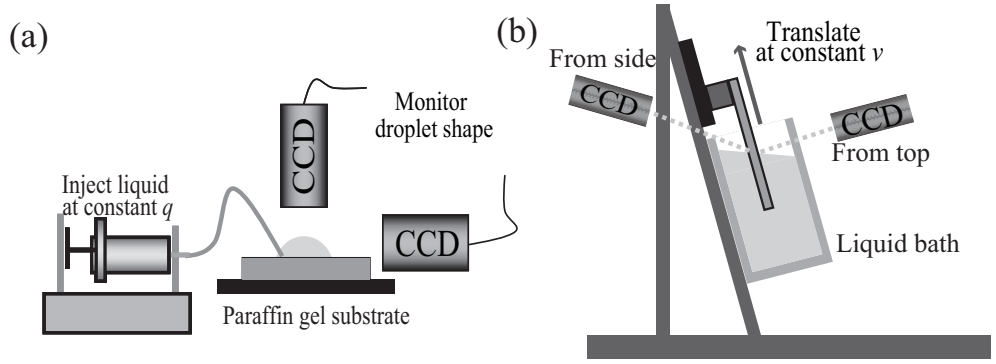

FIG. 5: Schematics of the wetting experiments on paraffin gels: **(a)** inflation of sessile droplets and **(b)** dip coating.

3.2 Results

Figure 6(a) shows sequential pictures and 6(b) shows the plot of radius and contact angle of a water droplet being inflated on a SBS-paraffin gel of c_{pol} = 10% at an inflation rate q = 20 μl/min. During the inflation process, the droplet contact line exhibits continuous and stick-slip motions. At an early stage of the inflation process ($t < 160$ s) while the droplet radius R is still sufficiently small ($R < 2$ mm), the contact line advances continuously at a nearly constant contact angle of order 100°. As R becomes large at a later stage ($t > 160$ s, $R > 2$ mm), the contact line starts the stick-slip motion, i.e., the droplet radius R stays at the same value during a certain moment and then suddenly increases. Looking at the contact angle, once the contact line sticks, θ starts to increase. At the moment θ reaches a critical value of order 100°, the contact line slips forward. Successively, the contact line repeats this stick-slip motion. After the inflation process, the water droplet was removed quickly and a picture of the gel surface was taken as shown in Fig. 6(c). The contact line leaves multiple circular traces on the gel surface.

In the dip-coating experiment, the contact line also exhibits a stick-slip behavior. Pictures of the contact line motion are shown in Fig. 7(a), and the plots of contact line position and contact angle are shown in Fig. 7(b). A gel of c_{pol} = 10% is used and the translation velocity v is fixed at 0.01 mm/s. In the dip coating, the stick-slip motion is more periodic. While the substrate is withdrawn from the liquid bath, the contact line is pinned until θ reaches a critical value close to 40°, and then the contact line slips down over a distance approximately 1 mm and θ goes back to a value of order 70°. After the slip, it is observed that the contact line leaves a straight line trace on the gel surface.

For a quantitative analysis, we conducted the inflating experiments of water droplets for various volume rates q ranging from from 1 μL/min to 200 μL/min. Figure 8(a) summarizes the contact line behavior at various R and q.

(i) At high q (e.g., 200 μL/min), the contact line advances continuously with a constant contact angle during the whole inflation process.

(ii) At intermediate q (e.g., 20 μL/min), the contact line initially exhibits the continuous advancing motion. As the droplet radius reaches a critical value ($R \approx 2.2$ mm), the contact line starts the stick-slip motion.

(iii) At low q (e.g., 2 μL/min), the contact line exhibits the stick-slip motion even at a very early stage of the inflation. However, when the droplet radius increases, now the contact line stops the stick-slip motion and starts to advance continuously again.

The same kinds of transitions of the contact line motions (continuous–stick-slip–continuous) were observed in dip coating by varying the translation velocity from 2 mm/s to 0.1 μm/s.

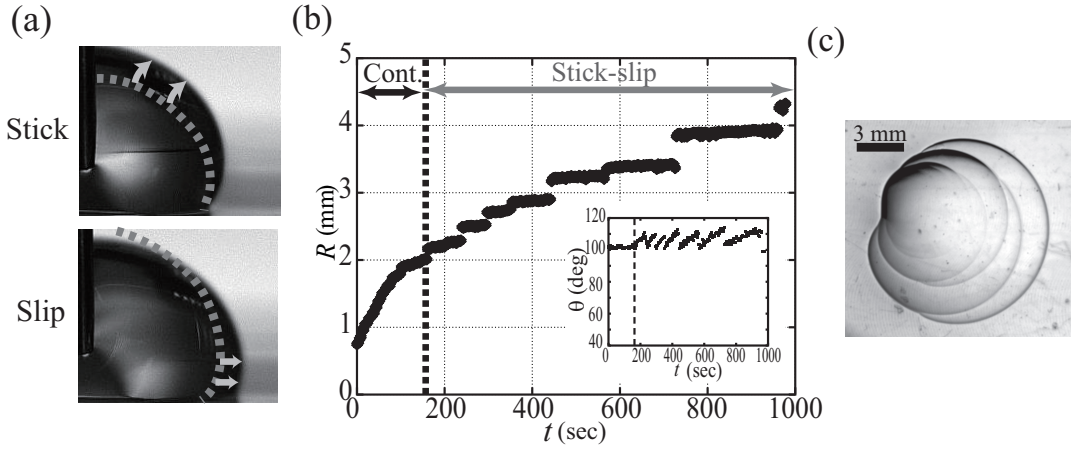

FIG. 6: (a) Stick-slip behavior of the contact line observed in an advancing droplet on SBS–paraffin gel of c_{pol} = 10% at an inflation rate q = 20 μL/min. **(b)** Plot of the radius and contact angle of the same droplet. **(c)** Multicircular traces formed on the gel surface after the inflation experiment.

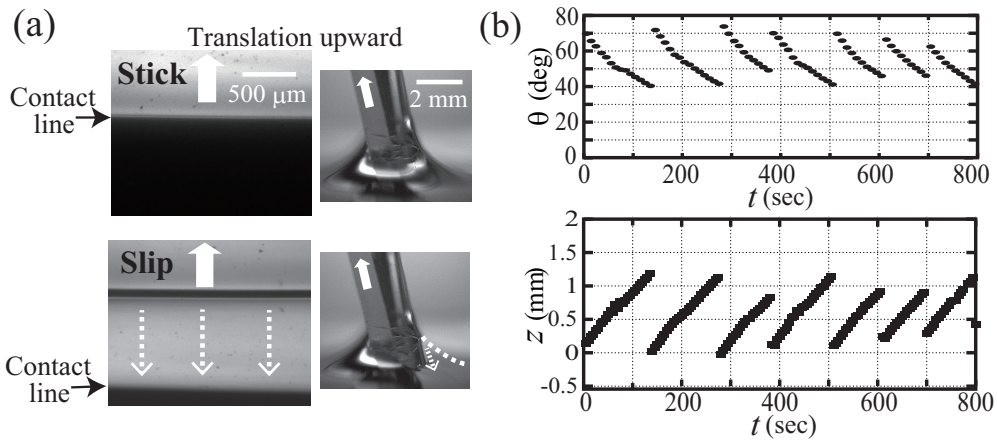

FIG. 7: (a) Stick-slip behavior of the contact line observed in dip coating on SBS–paraffin gel of c_{pol} = 10% at a translation velocity v = 0.01 mm/s. The front and side views of the liquid meniscus are shown. While the substrate is withdrawn from the liquid bath at a constant velocity, the contact line of the meniscus is pinned and then suddenly slips down over a distance of approximately 1 mm. **(b)** Plots of the contact line position and contact angle.

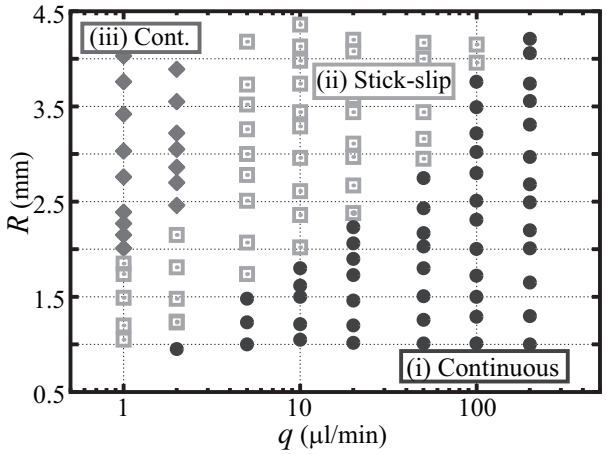

FIG. 8: Diagram of contact line behaviors as a function of droplet radius R and inflation rate q.

To explore the local deformation of the gel surface at the contact line, we conducted a supplemental experiment. A sessile droplet of volume 7.5 μL was placed on an SBS–paraffin gel and the surface profile near the contact line was measured by an optical profiler (Microsurf 3D, Fogal Nanotech, France). Figure 9 shows the surface profiles of gels (c_{SBS} = 10%) at times t = 2, 6, and 10 min.

The gel surface is pulled up and a ridge is formed at the contact line. Since there is no volume exchange between the droplet and the gel, the surface ridge is considered due to the balance between the vertical component of the liquid surface tension and the elastic resistance of the gel in analogy with the wetting problem on elastomer. In Carré et al. (1996); Shanahan (1987), Shanahan et al. predicted that the elastic surface ridge due to the capillary force has a logarithmic profile that typically leads to

$$\xi(x) \approx \frac{\gamma \sin\theta}{2\pi G} \ln\left(\frac{d}{|x|}\right), \tag{11}$$

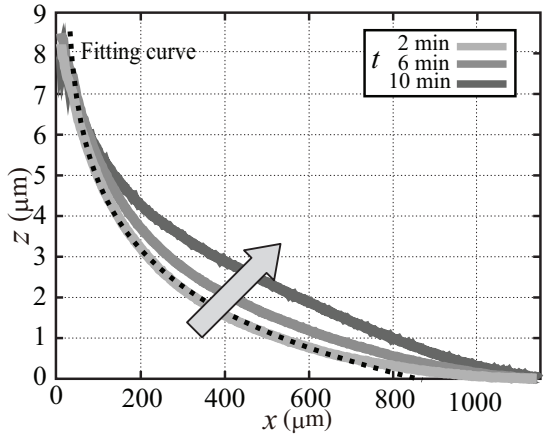

FIG. 9: Cross sections of the gel surface profiles close to the static contact line and its time evolution. A curve of the logarithmic fitting is superposed as a dashed line.

where G is a shear modulus of the gel, θ is a droplet contact angle, γ is the surface tension of water, $\approx$ 72 mN/m, and d indicates the macroscopic cutoff length of the surface ridge.

In Fig. 9, the profile fits well with the logarithmic curves at 2 min after the deposition. Meanwhile, the profile of the surface ridge is not persistent. If the contact line stays at the same position on the SBS–paraffin gel, the foot of the surface ridge gradually expands outward and the profile of the ridge becomes less steep.

3.3 Discussion

In order to compare the contact line behavior in Fig. 8 with the gel rheology, we further estimate the characteristic frequency of the contact line motion defined as

$$f = \frac{v_a}{R} \approx \frac{q}{2\pi R^3}, \tag{12}$$

where v_a is the apparent mean contact line velocity at given R and q, and f is the inverse of the typical period at which the contact line moves over the size of the surface deformation R at a velocity v_a. (Here we used R as the size of the surface deformation, as in Fig. 9, the width of the surface ridge is of the same order of drop radius.)

In Fig. 10(a), we replot the diagram as a function of f. It is clearly observed that the three regimes of the contact line motions (i)–(iii) are defined by f with two critical frequencies which characterize the transition: f_{c1} separates the (i) continuous advancing motion at a high frequency and (ii) stick-slip regime, and f_{c2} separates the (ii) stick-slip and (iii) continuous advancing at a low frequency. From the comparison with the measurement of gel rheology, it is also observed that the crossover frequency f_{cross} where the storage and loss modulus correspond with each other, G''/G' = 1, is between these two critical frequencies. Figure 10(b) shows the plot of two critical frequencies f_{c1} and f_{c2} on gels for various c_{pol} ranging from 8% to 20%. With the change of f_{cross}, the values of two critical frequencies vary dramatically.

We have conjectured that the observed contact line motions (continuous–stick-slip–continuous) are the consequence of the mechanical response of the gel to the capillary force applied at the contact line (Long et al., 1996). The transition of the contact line motions (i)–(iii) can be understood in terms of the characteristic frequency f, as schematized in Fig. 11.

– Regime (i): When the contact line advances quickly and the characteristic frequency is high ($f \gg f_{cross}$), the gel substrate responds as an elastic solid to the motion of the contact line. In this situation, the surface

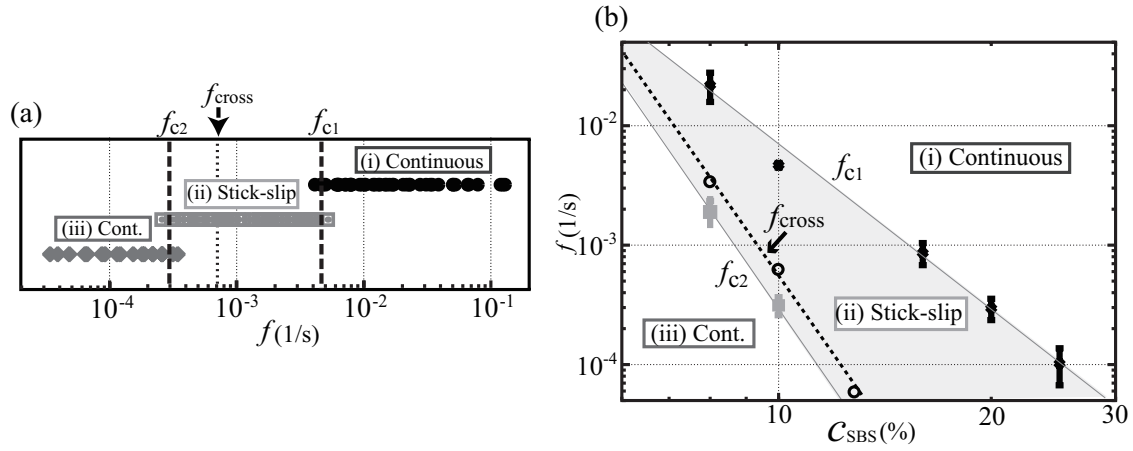

FIG. 10: (a) Replot of the data in Fig. 8 against the characteristic frequency f. The gel crossover frequency is also shown in the figure. **(b)** Plot of the two critical frequencies f_{c1} and f_{c2} against SBS concentration of gel c_{SBS}.

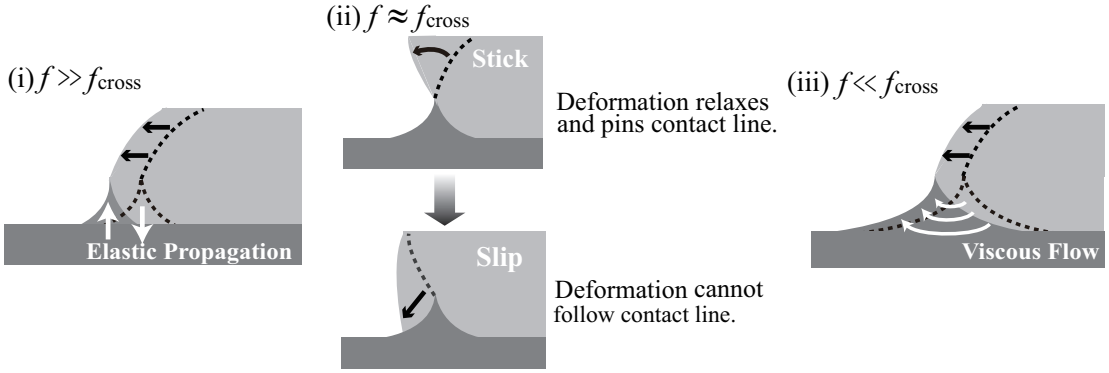

FIG. 11: Behaviors of the contact line and of gel surface deformation at different regimes (i)–(iii).

deformation at the contact line is an elastic ridge pulled by the surface tension of the liquid, which propagates with the motion of the contact line, resulting in the continuous advancing motion.

– Regime (ii): As the contact line velocity decreases and f comes close to the crossover frequency ($f \approx f_{cross}$), now the response of the gel surface is not purely elastic. The elastic resistance of the gel already starts to relax and a part of the surface deformation becomes irreversible. The surface ridge at the contact line behaves something like a "surface defect" that pins the contact line, resulting in the stick-slip motion.

– Regime (iii): In the other extreme situation, when the contact line advances slowly and f is sufficiently low ($f \ll f_{cross}$), the deformation of the gel surface totally relaxes until the contact line moves over a distance of order R. In this case, the gel substrate behaves nearly like a sheet of very viscous liquid with respect to the contact line motion Burton et al. (2010). With the movement of the contact line, a capillary flow is driven below the gel surface. The surface deformation is transported forward by this capillary flow, following the motion of the contact line. Therefore, the contact line exhibits a continuous advancing motion again.

In the stick-slip regime (ii), we propose a qualitative modelling that allows prediction of the link between jumps of the radius and jumps of the apparent contact angle, inspired by the model of wetting hysteresis on elastomer by

Extrand and Kumagai (1996). The schematic of our model is depicted in Fig. 12(a). The variables R_b, θ_b and R_a, θ_a are the droplet radii and apparent contact angles before and after the contact line slips on the surface ridge, and ϕ indicates the local slope of the ridge. Considering that the droplet volume V is conserved, the relations of droplet radii and contact angles are expressed as

$$V = \frac{\pi R_b^3}{3}(2 - 3\cos\theta_b) = \frac{\pi R_a^3}{3}(2 - 3\cos\theta_a). \tag{13}$$

We suppose that θ_a is an advancing contact angle on an undeformed surface and that the difference between θ_b and θ_a is essentially due to the local surface slope. To advance on a inclined surface, the contact line has to take an advancing angle equal to

$$\theta_b = \phi + \theta_a. \tag{14}$$

As θ_a is close to 90° in our situation, the Eqs. (13) and (14) are rewritten as a function of the ratio of two radii:

$$\left(\frac{R_a}{R_b}\right)^3 = \frac{2 - 3\cos(\theta_a + \phi)}{2 - 3\cos\theta_a}, \tag{15}$$

$$\approx 1 + \frac{3}{2}\Big[\cos\theta_a - \cos(\theta_a + \phi)\Big]. \tag{16}$$

With an approximation that ϕ is sufficiently small, the ratio R_a/R_b relates to ϕ as shown in the following expression:

$$\frac{R_a}{R_b} \approx 1 + \frac{\phi}{2}. \tag{17}$$

This equation links the ratio of successive droplet radii to the local surface slope ϕ:

$$\phi = \frac{2(R_a - R_b)}{R_b} = 2\frac{\Delta R}{R_b}. \tag{18}$$

In order to check this model, we used the experimental data of c_{SBS} = 10% in the stick-slip regime (ii) and calculated the quantity $2\Delta R/R_b$ for various stick-slip motions. In Fig. 12(b), we compared it to the value of $\phi = \theta_b - \theta_a$ extracted from the direct measurement of the contact angle θ. Both quantities are noted nearly equal, which indicates that our model has captured the essential features successfully.

Let us close this section by discussing the fact that ϕ remains locked at the value 10° independently of f. These results are a bit surprising, because in available modeling in Eq. (11) (Carré et al., 1996; Shanahan, 1987), the local slope of the surface ridge $h'(x)$ depends on the elastic modulus G and thus, here, indirectly on f, and even diverges

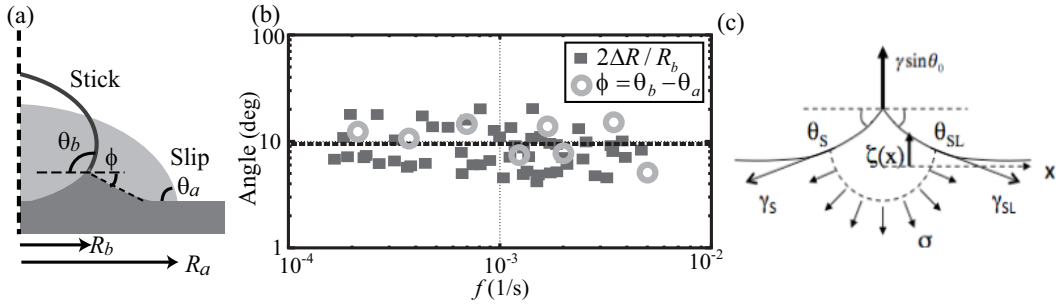

FIG. 12: (a) Parameters for the geometric considerations in the stick-slip regime. **(b)** Plot of the angle of the local slope of the gel surface predicted from the ratio of successive droplet radii $2\Delta R/R_b$ against f. For comparison, the value of $\phi = \theta_b - \theta_a$ directly obtained from the contact angle measurement was plotted as hollow circles. **(c)** Distortions induced by the normal component, that is moderated by both elastic stresses and substrate surface tensions.

near $x = 0$. All seems here to happen as if ϕ would be selected by some truncation of this profile at a small scale, eliminating the contribution of G. In recent studies of wetting on elastomer, this truncation was proposed to be ruled by the surface tension of the substrate (Jerison et al., 2011; Marchand et al., 2012; Style and Dufresne, 2012). In particular, one of us (L. Limat) modified Shanahan's approach by means of the substrate surface tension γ_s (Limat, 2012). In its simplest form, for a contact angle of 90°, the expression of $\xi(x)$ is given as

$$\xi(x) \approx \frac{\gamma \sin\theta}{2\pi G} \ln\left(\frac{d + l_e}{|x| + l_e}\right), \tag{19}$$

where $l_e = \gamma_s/G$ is the elastocapillary length. The present approach indicates that when the substrate surface tension is taken into account, this logarithmic is still valid but shifts a distance equal to l_e, which "cuts" the divergence at this scale, connecting to the Neumann equilibrium at $x = 0$ [Fig. 12(c)]:

$$2\gamma_s\theta_s = \gamma \sin\theta, \tag{20}$$

where θ_s is the local slope of the surface ridge.

For a paraffin gel, the typical value of γ_s is 30 mN/m (Queimada et al., 2001; Talreja et al., 2012), giving the value of $l_e \approx 6$ μm for G = 5 kPa. Indeed, we have checked experimentally by profilometry (Fig. 9) that a slope of order 10° of the substrate is reached at approximately 10 μm from the contact line, which is quite close to the expected value for l_e. In addition, the profile of the surface in the vicinity of the contact line (10 μm $\leq x \leq$ 50 μm) does not evolve significantly within our time window. From these remarks, it is quite natural that ϕ does not depend on f.

Note, however, that this model has also a prediction for ϕ, whose simplest form is $\phi = \theta_s$ when the two substrate surface tensions (dry and wetted) are equal. In our case, there is a problem with this approximation, as with the value obtained from the literature for γ_s (γ_s = 30 mN/m), one has $\gamma > 2\gamma_s$. This means that Neumann equilibrium also cannot be satisfied at the contact line. Furthermore, we should consider the balance of forces in asymmetric situations, as in our experiment, the advancing and receding angles are different from 90°.

Although the models for the wetting on elastomer cannot be applied directly here, as the paraffin gel is viscoelastic and the three interfacial tensions cannot be balanced in our situation, our results suggest that one of their main predictions, i.e., the relevance of elastocapillary length at small scale, could also hold in this very complex system.

4. CONCLUSION

In this paper we report the dynamics of a liquid contact line on gel substrates: hydrophilic PAMPS–PAAM gel and hydrophobic SBS–paraffin gels. In both situations, different gel characteristics dramatically affect the contact line behavior.

On hydrophilic PAMPS–PAAM gels, the contact line of the sessile droplet successively exhibits two different regimes: pinned and receding. The contact line is initially pinned after the droplet is placed. As the water diffusion proceeds, the effective contact angle of the droplet decreases while the local slope of the gel surface near the contact line increases. Finally, these two angles almost correspond to each other, and it is at this moment that the contact line starts to recede. Therefore, at the moment of the contact line recession, the actual contact angle is nearly 0°. Regarding the mechanism of the pinning–receding transitions, we have proposed a physical model that the diffusive flux of the liquid forms a locally swollen region at the contact line, and whether the contact line is pinned or receded is determined by the wetting property of this swollen region. This model correctly explains the effect of the gel swelling ability on the length of the initial pinned regime.

On hydrophobic SBS–paraffin gels, we have observed that the droplet contact line exhibits three different regimes of motions, and their transition is characterized by a frequency f determined by the apparent contact line velocity v and droplet radius R as $f = v/R$. At high f with respect to the crossover frequency of gel f_{cross}, the contact line moves continuously with a constant contact angle. As the contact line slows down and f approaches f_{cross}, the contact line starts the stick-slip motion: the contact line is pinned, then suddenly slips forward. At f sufficiently lower than f_{cross}, the contact line stops stick-slip and advances continuously again. We have conjectured that the observed transitions of the contact line motions (continuous–stick-slip–continuous) are the consequence of the gel rheology

affecting the dynamics of the contact line. Depending on the frequency, the behavior of the liquid contact line on gels shows both aspects of wetting on elastic solids and on viscous liquid sheets. At an intermediate frequency where the gel behaves like neither a solid nor liquid, the stick-slip motion appears.

Our results show that the dynamics of the contact line on gel substrates are quite different from those observed for general solid materials, especially for the appearance of the different regimes of motions. Although our experimental and theoretical approaches have grasped essential features, further studies are still required for a detailed understanding. For wetting on hydrophilic gels, theoretical and numerical modellings which predict the pinned–receding transition of the contact line should be realized. This requires the combined equations of the water volume transport from the droplet to the gel and of the balance of interfacial tensions at the contact line to be solved. Alternatively, experimental investigations of the gel surface tension are needed to provide a precise parameter for these modellings (Yoshitake et al., 2008). For hydrophobic gels, elaborated models based on those for the wetting on elastomer should be developed. Here, we address more complex situations. As the gel has a viscoelastic response, two types of deformations are superposed in the gel surface ridge: reversible (elastic) and irreversible (plastic). Furthermore, the three interfacial tensions are not balanced ($\gamma > 2\gamma_s$) in certain cases. These problems are noted as among the important future directions in wetting science.

ACKNOWLEDGMENTS

The authors gratefully thank G. Ducouret and A. Chateauminois (ESPCIParisTech) for their support with regard to the rheology and surface profile measurements, as well as Y. Shimokawa, K. Sakai (University of Tokyo), and M. Doi (Beihang University) for fruitful discussions. The funding of T.K. has been covered by the Labex SEAM.

REFERENCES

Aradian, A., Raphael, E., and de Gennes, P. G., Dewetting on porous media with aspiration, *Eur. Phys. J. E: Soft Matter Biol. Phys*., vol. **2**, pp. 367–376, 2000.

Bacri, L. and Wyart, F. B., Droplet suction on porous media, *Eur. Phys. J. E: Soft Matter Biol. Phys*, vol. **3**, pp. 87–97, 2000.

Banaha, M., Daerr, A., and Limat, L., Spreading of liquid drops on Agar gels, *Eur. Phys. J. Special Topics*, vol. **166**, pp. 185–188, 2009.

Baumberger, T., Caroli, C., and Martina, D., Solvent control of crack dynamics in a reversible hydrogel, *Nature Mat.*, vol. **5**, pp. 552–555, 2006.

Bonn, D., Eggers, J., Indekeu, J., Meunier, J., and Rolley, E., Wetting and spreading, *Rev. Mod. Phys.*, vol. **81**, pp. 739–805, 2009.

Burton, J. C., Huisman, F. M., Alison, P., Rogerson, P., and Taborek, P., Experimental and numerical investigation of the equilibrium geometry of liquid lenses, *Langmuir*, vol. **26**, pp. 15316–15324, 2010.

Cámara, R. P., Best, A., Butt, H. J., and Bonaccurso, E., Effect of capillary pressure and surface tension on the deformation of elastic surfaces by sessile liquid microdrops: An experimental investigation, *Langmuir*, vol. **24**, no. 19, pp. 10565–10568, 2008.

Cámara, R. P., Auernhammer, G. K., Koynov, K., Lorenzoni, S., Raiteri, R., and Bonaccurso, E., Solid-supported thin elastomer films deformed by microdrops, *Soft Matter*, vol. **5**, pp. 3611–3617, 2009.

Carré, A. and Shanahan, M. E. R., Viscoelastic braking of a running drop, *Langmuir*, vol. **17**, no. 10, pp. 2982–2985, 2001.

Carré, A., Gastel, J. C., and Shanahan, M. E. R., Viscoelastic effects in the spreading of liquids, *Nature*, vol. **379**, pp. 432–434, 1996.

Daniels, K. E., Mukhopadhyay, S., Houseworth, P. J., and Behringer, R. P., Instabilities in droplets spreading on gels, *Phys. Rev. Lett.*, vol. **99**, no. 12, paper 124501, 2007.

de Gennes, P. G., Wyart, F. B., and Quere, D., *Capillarity and Wetting Phenomena*, Springer, New York, 2003.

Deegan, R. D., Bakajin, O., Dupont, T. F., Huber, G., Nagel, S. R., and Witten, T. A., Contact line deposits in an evaporating drop, *Phys. Rev. E: Stat., Nonlinear, Soft Matter Phys.*, vol. **62**, pp. 756–765, 2000.

Doi, M., Gel dynamics, *J. Phys. Soc. Jpn.*, vol. **78**, paper 052001, 2009.

Extrand, C. W. and Kumagai, Y., Contact angles and hysteresis on soft surfaces, *J. Colloid Interface Sci.*, vol. **184**, pp. 191–200, 1996.

Fermigier, M., Limat, L., Wesfreid, J. E., Boudinet, P., and Quilliet, C., Two-dimensional patterns in Rayleigh-Taylor instability of a thin layer, *J. Fluid Mech.*, vol. **236**, pp. 349–383, 1992.

Gong, J. P., Kurokawa, T., Narita, T., Kagata, G., Osada, Y., Nishimura, G., and Kinjo, M., Synthesis of hydrogels with extremely low surface friction, *J. Am. Chem. Soc.*, vol. **123**, no. 23, pp. 5582–5583, 2001.

Holmes, D. P., Roché, M., Sinha, T., and Stone, H. A., Bending and twisting of soft materials by non-homogenous swelling, *Soft Matter*, vol. **7**, pp. 5188–5193, 2011.

Hu, H. and Larson, R. G., Evaporation of a sessile droplet on a substrate, *J. Phys. Chem. B*, vol. **106**, pp. 1334–1344, 2002.

Hu, X., Hao, L., Wang, H., Yang, X., Zhang, G., Wang, G., and Zhang, X., Hydrogel contact lens for extended delivery of ophthalmic drugs, *Int. J. Pol. Sci.*, vol. **2011**, paper 814163, 2011.

Jerison, E. R., Xu, Y., Wilen, L. A., and Dufresne, E. R., Deformation of an elastic substrate by a three-phase contact line, *Phys. Rev. Lett.*, vol. **106**, paper 186103, 2011.

Kajiya, T., Daerr, A., Narita, T., Royon, L., Lequeux, F., and Limat, L., Dynamics of the contact line in wetting and diffusing processes of water droplets on hydrogel (PAMPS–PAAM) substrates, *Soft Matter*, vol. **7**, pp. 11425–11432, 2011.

Kajiya, T., Daerr, A., Narita, T., Royon, L., Lequeux, F., and Limat, L., Advancing liquid contact line on visco-elastic gel substrates: Stick-slip vs. continuous motions, *Soft Matter*, vol. **9**, pp. 454–461, 2013.

Kaneko, D., Tada, T., Kurokawa, T., Gong, J. P., and Osada, Y., Mechanically strong hydrogels with ultra-low frictional coefficients, *Adv. Mater.*, vol. **17**, pp. 535–538, 2005.

Kobayashi, M., Makino, M., Okuzono, T., and Doi, M., Interference effects in the drying of polymer droplets on substrate, *J. Phys. Soc. Jpn.*, vol. **79**, paper 044802, 2010.

Kundakci, S., Üzum, Ö., and Karada, E., Swelling and dye sorption studies of acrylamide/2-acrylamido-2-methyl-1-propanesulfonic acid/bentonite highly swollen composite hydrogels, *Reac. Func. Polym.*, vol. **68**, pp. 458–473, 2008.

Kurata, J., Grattan, K. T. V., Uchiyama, H., and Tanaka, T., Water surface measurement in a shallow channel using the transmitted image of a grating, *Rev. Sci. Instrum.*, vol. **61**, pp. 736–739, 1990.

Landau, L. D. and Lifshitz, E. M., *Theory of Elasticity*, 3rd ed., Butterworth Heinemann, 1986.

Limat, L., Straight contact lines on a soft, incompressible solid, *Eur. Phys. J. E: Soft Matter Biol. Phys.*, vol. **35**, paper 134, 2012.

Long, D., Ajdari, A., and Leibler, L., How do grafted polymer layers alter the dynamics of wetting?, *Langmuir*, vol. **12**, pp. 1675–1680, 1996.

Lopes, M. C. and Bonaccurso, E., Evaporation control of sessile water drops by soft viscoelastic surfaces, *Soft Matter*, vol. **8**, pp. 7875–7881, 2012.

Marchand, A., Das, S., Snoeijer, J. H., and Andreotti, B., Capillary pressure and contact line force on a soft solid, *Phys. Rev. Lett.*, vol. **108**, paper 094301, 2012.

Matsuo, E. S. and Tanaka, T., Patterns in shrinking gels, *Nature*, vol. **358**, pp. 482–485, 1992.

Morishita, M., Kobayashi, M., Yamaguchi, T., and Doi, M., Observation of spatio-temporal structure in stick-slip motion of an adhesive gel sheet, *J. Phys. Condens. Matter*, vol. **22**, no. 36, paper 365104, 2010.

Nonomura, Y., Morita, Y., Hikima, T., Seino, E., Chida, S., and Mayama, H., Spreading behavior of water droplets on fractal Agar gel surfaces, *Langmuir*, vol. **26**, pp. 6150–16154, 2010.

Nonomura, Y., Chida, S., Seino, E., and Mayama, H., Anomalous spreading with Marangoni flow on Agar gel surfaces, *Langmuir*, vol. **28**, pp. 3799–3806, 2012.

Peppas, N. A., Bures, P., Leobandung, W., and Ichikawa, H., Hydrogels in pharmaceutical formulations, *Eur. J. Pharm. Biopharm.*, vol. **50**, pp. 27–46, 2000.

Pu, G. and Severtson, S. J., Characterization of dynamic stick-and-break wetting behavior for various liquids on the surface of a highly viscoelastic polymer, *Langmuir*, vol. **24**, pp. 4685–4692, 2008.

Pu, G., Ai, J., and Severtson, S. J., Drop behavior on a thermally-stripped acrylic polymer: Influence of surface tension induced wetting ridge formation on retention and running, *Langmuir*, vol. **26**, pp. 12696–12702, 2010.

Queimada, A. J., Marrucho, I. M., and Coutinho, J. A. P., Surface tension of pure heavy n-alkanes: A corresponding states approach, *Fluid Phase Equilib.*, vols. **183–184**, pp. 229–238, 2001.

Roman, B. and Bico, J., Elasto-capillarity: Deforming an elastic structure with a liquid droplet, *J. Phys.: Condens. Matter.*, vol.

22, paper 493101, 2010.

Shanahan, M. E. R., The influence of solid micro-deformation on contact angle equilibrium, *J. Phys. D: Appl. Phys.*, vol. **20**, pp. 945–950, 1987.

Shanahan, M. E. R. and de Gennes, P. G., The ridge produced by a liquid near the triple line solid/liquid/fluid, *C. R. Acad. Sci. Paris*, Ser. II, vol. **302**, pp. 517–521, 1986.

Style, R. W. and Dufresne, E. R., Static wetting on deformable substrates, from liquids to soft solids, *Soft Matter*, vol. **8**, pp. 7177–7184, 2012.

Suzuki, A. and Tanaka, T., Phase transition in polymer gels induced by visible light, *Nature*, vol. **346**, pp. 345–347, 1990.

Szabó, D., Akiyoshi, S., Matsunaga, T., Gong, J. P., and Osada, Y., Spreading of liquids on gel surfaces, *J. Chem. Phys.*, vol. **113**, pp. 8253–8259, 2000.

Talreja, M., Kusaka, I., and Tomasko, D. L., Analyzing surface tension in higher alkanes and their CO_2 mixtures, *Fluid Phase Equilib.*, vol. **319**, pp. 67–76, 2012.

Yang, J., Yamato, M., Kohno, C., Nishimoto, A., Sekine, H., Fukai, F., and Okano, T., Cell sheet engineering: Recreating tissues without biodegradable scaffolds, *Biomaterials*, vol. **26**, no. 33, pp. 6415–6422, 2005.

Yoshitake, Y., Mitani, S., Sakai, K., and Takagi, K., Surface tension and elasticity of gel studied with laser-induced surface-deformation spectroscopy, *Phys. Rev. E: Stat., Nonlinear, Soft Matter Phys.*, vol. **78**, paper 041405, 2008.